Manuscript prepared for Atmos. Chem. Phys.
with version 2014/07/29 7.12 Copernicus papers of the LaTeX class copernicus.cls.
Date: 25 March 2017

Secondary ozone peaks in the troposphere over the Himalayas

Narendra Ojha[1], Andrea Pozzer[1], Dimitris Akritidis[1,2], and Jos Lelieveld[1,3]

[1]Atmospheric Chemistry Department, Max Planck Institute for Chemistry, Mainz, Germany
[2]Department of Meteorology and Climatology, School of Geology, Aristotle University of Thessaloniki, Thessaloniki, Greece
[3]Energy, Environment and Water Research Center, The Cyprus Institute, Nicosia, Cyprus

Correspondence to: Narendra Ojha (narendra.ojha@mpic.de)

1   **Abstract.** Layers with strongly enhanced ozone concentrations in the middle-upper troposphere,

2   referred to as Secondary Ozone Peaks (SOPs), have been observed in different regions of the world.

3   Here we use the global ECHAM5/MESSy atmospheric chemistry model (EMAC) to (i) investigate

4   the processes causing SOPs, (ii) explore both their frequency of occurrence and seasonality, and (iii)

5   assess their effects on the tropospheric ozone budget over the Himalayas. The vertical profiles of

6   potential vorticity (PV) and a stratospheric ozone tracer (O_3s) in EMAC simulations, in conjunction

7   with the structure of SOPs, suggest that SOPs over the Himalayas are formed by Stratosphere-to-

8   Troposphere Transport (STT) of ozone. The spatial distribution of O_3s further shows that such effects

9   are in general most pronounced in the northern part of India. Model simulated ozone distributions

10 and backward air trajectories show that ozone rich air masses, associated with STT, originate as

11 far as northern Africa and the North Atlantic Ocean, the Middle-East, as well as nearby regions in

12 Afghanistan and Pakistan, and are rapidly (within 2–3 days) transported to the Himalayas. Analysis

13 of a 15-year (2000-2014) EMAC simulation shows that the frequency of SOPs is highest during the

14 pre-monsoon season (e.g. 11% of the time in May), while no intense SOP events are found during

15 the July-October period. The SOPs are estimated to enhance the Tropospheric Column Ozone (TCO)

16 over the central Himalayas by up to 21%.

17 **1   Introduction**

18 Tropospheric ozone is a short-lived climate forcer (Shindell et al., 2012) and an air pollutant with

19 adverse effects on human health and crop yields (Monks et al., 2015, and references therein). The

20 effects of tropospheric ozone on crop yields and human health occur near the surface, whereas its

21 radiative forcing is shown to be strongest in the middle-upper troposphere (e.g. Lacis et al., 1990;

Myhre et al., 2013; Monks et al., 2015). The processes controlling tropospheric ozone in the middle and upper troposphere can be different from those near the surface. The photochemistry involving non-methane volatile organic compounds (NMVOCs) and carbon monoxide, in the presence of nitrogen oxides (NOx) primarily controls ozone pollution in the planetary boundary layer. In contrast, dynamics involving Stratosphere-Troposphere Exchange (STE) play a key role in the middle-upper troposphere (e. g. Holton and Lelieveld, 1996; Lelieveld and Dentener, 2000; Neu et al., 2014; Ojha et al., 2014; Monks et al., 2015). Therefore, to quantify the relative contributions of photochemical and dynamical processes to the ozone budget and assess the climatic impacts of anthropogenic ozone, studies of the vertical distribution of ozone are essential.

Ozone observations have been conducted globally and locally using different instruments and platforms as reviewed recently by Tanimoto et al. (2015). Balloon-borne observations employing ozonesondes offer the advantage of measuring ozone across the tropopause. Analyses of ozonesonde observations have provided valuable information on the variability, general features and trends in ozone profiles (e.g. Logan, 1985, 1994). Secondary maxima in ozone profiles, called Secondary Ozone Peaks (SOPs), are a unique phenomenon in which anomalously large ozone concentrations are observed in confined layers in the middle-upper troposphere or lower stratosphere.

The occurrences of SOPs, underlying processes and their global distribution have been discussed in a limited number of studies (Dobson, 1973; Reid and Vaughan, 1991; Varotsos et al., 1994), reviewed by Lemoine (2004). SOPs have been commonly observed in high latitudes, for example, as laminated structures of ozone with the highest frequency of occurrence during the spring season (Dobson, 1973). These laminated structures are primarily considered to be a winter-spring phenomenon, with a peak altitude of occurrence near 14 km (Reid and Vaughan, 1991). Varotsos et al. (1994) suggested that the north and northwest atmospheric circulations in the lower stratosphere play a key role in the formation of SOPs observed over Athens, Greece. Overall, the occurrence of SOPs is typically considered to be a northern hemispheric phenomenon, with no SOPs reported in the tropics and the southern hemisphere (Lemoine, 2004). Trickl et al. (2011) showed the influences of ozone import from the stratosphere and transport along the subtropical jet stream over Europe. According to the aforementioned studies, SOPs are mainly attributed to dynamical processes involving STE, advection and Rossby wave breaking events.

Recent studies (Hwang et al., 2005, 2007; Park et al., 2012) focusing on the Korean region showed that SOP events regularly occur over mid-latitudes. In contrast to earlier studies that demonstrated the occurrence of SOPs mostly in the lower stratosphere, several SOPs were observed in the upper troposphere over Korea. Hwang et al. (2005) attributed these SOPs to the downward transport of ozone from the stratosphere on a timescale of about one day (24 h), typical of cross-tropopause exchange. Furthermore, the frequency of occurrence, estimated from 9 years of ozonesonde observations, was found to have strong seasonal variability over Korea with a broad winter-spring maxima and frequencies of occurrence up to 50–80 % (Hwang et al., 2005). Moreover, Hwang et al. (2005)

reported an increase in SOP occurrences over Korea, while the STT effects are anticipated to increase tropospheric ozone in the future (Banerjee et al., 2016).

The studies pertaining to the influences of STT on the vertical profiles of ozone are relatively sparse over the tropical Indian region. Mandal et al. (1998) analyzed observations from ozonesondes and an MST Radar, and attributed the enhanced ozone mixing ratios in the upper troposphere to STT through the indistinct tropopause over southern India. Fadnavis et al. (2010) combined satellite-borne measurements (TES and MLS) with simulations performed by the MOZART model and showed significant influences of STT over India in particular during winter and spring /pre-monsoon seasons. Venkat Ratnam et al. (2016) used satellite observations to estimate the effect of STE associated with tropical cyclones over the north Indian Ocean. Most of the studies based on in situ measurements have however been confined over the southern part of India (e.g. Mandal et al., 1998; Sinha et al., 2016) and the adjacent marine regions (Lal et al., 2013). Ganguly and Tzanis (2011) used ozonesonde observations from three Indian stations operated by the Indian Meteorological Department (IMD) and suggested that overall STT only plays a minor role into the budget of tropospheric ozone over India. However, the influences of STT were found to increase with latitude /northward over India (Ganguly and Tzanis, 2011).

Studies investigating the SOP structures and implications have been few over the tropical Indian region, until very recently (Ojha et al., 2014; Das et al., 2016). The events over southern India were found to be mainly associated with stratospheric intrusions during tropical cyclonic storms (Das et al., 2016). In contrast, the SOP events observed over the central Himalayas in northern India appear similar to what is typically observed over the mid-high latitudes as mentioned earlier. Moreover, SOPs were observed to be more frequent during spring, and were attributed to the combined effects of STE and advection (Ojha et al., 2014). In the previous work using weekly ozonesonde measurements (3–4 profiles per month), covering the period January 2011–December 2011 (Ojha et al., 2014), only 6 SOP events were observed, being insufficient to calculate the frequency and seasonality of SOP occurrences. Additionally, model simulations are required to both trace the source regions and quantify the effect of SOPs on the tropospheric ozone budget. Such investigations are of key importance as the Indo-Gangetic Plain (IGP) and Himalaya region are global hotspot regions in terms of anthropogenic pressures that could impose threats to Asia's water and food security (Ramanathan et al., 2008). Satellite-based studies corroborate the high pollution loading over northern India and the nearby IGP including the Tropospheric Column Ozone (TCO) over South Asia (Fishman et al., 2003). The IGP is a regional hotspot of the so called "Atmospheric Brown Clouds (ABC)", consisting of brown haze formed by sub-micron size aerosol particles, emitted from a wide range of anthropogenic and natural sources. It has been shown that ABC reduce the amount of sunlight reaching the Earth's surface by as much as 10 to 15%, and enhance atmospheric solar heating by as much as 50% (Ramanathan et al., 2007).

95   In the present study, the global atmospheric chemistry climate model EMAC (ECHAM5/MESSy

96 Atmospheric Chemistry) has been used to explore the processes causing the SOPs, investigate the

97 frequency and seasonality of their occurrence and finally assess their impact on the tropospheric

98 ozone budget over the central Himalayas.

99 **2   Methodology**

100 **2.1   EMAC**

101 The ECHAM5/MESSy Atmospheric Chemistry (EMAC) is a numerical system for the simulation

102 of regional and global air quality and climate (Jöckel et al., 2010). In this work the model results

103 from simulation RC1SD-base-10a of the ESCiMo project (Jöckel et al., 2016) are used. The general

104 circulation model ECHAM5 version 5.3.02 (Roeckner et al., 2006) and the Modular Earth Submodel

105 System (MESSy) version 2.51 (Jöckel et al., 2016) were used at T42L90MA-resolution, implying a

106 spherical truncation of T42 (corresponding to a quadratic Gaussian grid of approx. 2.8 by 2.8 degrees

107 in latitude and longitude) and 90 vertical hybrid pressure levels up to 0.01 hPa. The dynamics of

108 the general circulation model were weakly nudged by Newtonian relaxation towards ERA-Interim

109 reanalysis data (Dee et al., 2011). Gas-phase and particulate trace species calculated with the EMAC

110 model have been extensively evaluated in previous studies (e.g. Pozzer et al., 2007, 2010, 2012).

111 Simulation RC1SD-base-10a with model output every 10h, was selected between the ESCiMo sim-

112 ulations as suggested in Jöckel et al. (2016) ("For intercomparison with observations, we recommend

113 to use the results of [...] RC1SD-base-10a."). Detailed information on the model set-up and compar-

114 ison with observations can be found in Jöckel et al. (2016).

115   A tracer of stratospheric ozone, denoted as O_3s in EMAC, has been used to quantify the effects

116 of STT. O_3s follows the transport and destruction processes of ozone in the troposphere but not its

117 chemical formation (Roelofs and Lelieveld, 1997) and it is initialized to O_3 in the stratosphere.

118 **2.2   Tropopause height and tropopause folds**

119 The Lapse Rate Tropopause (LRT) height is calculated from EMAC output using the WMO defi-

120 nition as the altitude at which lapse rate decreases to a value of 2 °C/km or less, provided that the

121 average lapse rate between this level and all higher levels within the adjacent 2 km do not exceed 2

122 °C/km.

123   Tropopause folds in EMAC simulations were identified with an algorithm developed by Sprenger

124 et al. (2003), and improved by Ŝkerlak et al. (2014), using the three dimensional fields of potential

125 vorticity, potential temperature and specific humidity. The vertical extent of the folds, as determined

126 by the difference between the upper and middle tropopause crossings (see Fig. 1 in Tyrlis et al.

127 (2014)) has been further used to identify shallow, medium and deep folds, as described and used

128 elsewhere (Tyrlis et al., 2014; Ŝkerlak et al., 2015; Akritidis et al., 2016).

2.3 Observational dataset

The occurrence of SOPs was reported using ozonesonde observations from Nainital (79.45° E, 29.37° N, 1958 m asl), a high altitude station located in the central Himalayan region (Fig. 1;(Ojha et al., 2014)). These data have been used to evaluate the capability of EMAC to reproduce SOPs over this region. Some typical events of SOP occurrence over Nainital can be seen in Fig. 2. The ozone mixing ratios in the middle-troposphere (10–11 km) are clearly observed to be very high (150–250 nmol mol^{-1}) forming an SOP. The location of Nainital station and the geographical topography of the northern Indian region are also shown in Fig. 1.

Ozone profiles at Nainital were measured using Electrochemical Concentration Cell (ECC) ozoneson-des. The method utilizes the titration of ozone in potassium iodide solution, which leads to produc-tion of Iodine (I_2). The conversion of I_2 to I^- in the cell leads to the flow of two electrons for each ozone molecule entered. The measured cell current, flow rate of air along with sensor parameters, e.g. the background current and pump temperature, are used to derive ozone mixing ratios (Ojha et al., 2014). The precision and accuracy of ECC-ozonesondes are reported to be $\pm(3–5)\%$ and $\pm(5–10)\%$ respectively, up to 30 km altitude (Smit et al., 2007).

The yearlong observations analyzed previously (Ojha et al., 2014) showed six occurrences of ele-vated ozone layers in the 10–12 km altitude range, identified as SOPs. For the analysis of frequency of occurrence and impacts of SOPs, we classify an ozone profile as SOP, if 1) O_3 mixing ratios at 10–12 km, are higher by at least by 50% compared to average ozone in the lower troposphere and 2) O_3 mixing ratios are again lower (at least by 20%) above the SOP (as shown in Fig. 2 and described in more detail in the section 3.3).

Further details of the Nainital station and meteorology (Sarangi et al., 2014; Singh et al., 2016) and balloon-borne measurements (Smit et al., 2007; Ojha et al., 2014; Naja et al., 2016) can be found elsewhere.

2.4 Backward trajectories

We used the Hybrid Single Particle Lagrangian Integrated Trajectory (HYSPLIT) model (http://ready.arl.noaa.gov/HYSPLIT.php) to investigate the source regions and the transport patterns caus-ing SOPs over the central Himalayas. 5-day backward trajectories have been simulated at 10, 11 and 12 km above sea level (asl) (Fig. S4 in the supplement), which are the typical altitudes for the 6 SOP events shown in Fig. 2. Additional trajectories have been computed for each model timestep in the month of May 2002 (Fig. 6), during which the model predicts the highest frequency of occurrence in the 2000–2014 period. HYSPLIT trajectory simulations are driven by NCEP reanalysis meteorolog-ical fields and the model vertical velocity option has been used for the vertical motions. More details of the backward trajectory simulations using the HYSPLIT model (Draxler and Hess, 1997, 1998;

163 Draxler et al., 2014) and use of various datasets as meteorological inputs over the Indian region can

164 be found elsewhere (e.g. Ojha et al., 2012; Kumar et al., 2015).

3   Results and Discussion

3.1   Model Evaluation

167 Fig. 2 shows the comparison of EMAC simulated ozone profiles with ozonesonde measurements

168 over Nainital during six SOP events reported previously (Ojha et al., 2014). Model ozone fields have

169 been bilinearly interpolated to the observation site and model output closer to the time of observation

170 is weighted higher (Ojha et al., 2016). As the vertical resolution of EMAC simulations is about 500–

171 600 m in the middle troposphere (10–12 km), where SOPs are typically observed, the observational

172 values are also shown at similar vertical resolution for comparison. The average ozone mixing ratios

173 along with the corresponding standard deviations for the six events are compared between model

174 and observations in Table 1 for lower, middle and upper tropospheric altitudes.

175 The EMAC model is found capable of reproducing the altitudinal placement of the SOPs over the

176 central Himalayas during all six events. For example, on 20th Apr and 9th May the model shows the

177 peak ozone mixing ratios at 10.5 km asl, in agreement with the ozonesonde profiles. On other events,

178 such as on 11th Feb, 10th Mar and 25th Oct, the altitude of SOP differs slightly (by 0.5-1 km) between

179 model and ozonesonde profiles, except on 7th Jun (by 2 km). The aforementioned discrepancies in

180 the altitude of SOPs occurrence might be related to the model vertical resolution.

181 In addition to the altitude of SOPs occurrence, EMAC also quantitatively captures the ozone en-

182 hancements. The model bias in simulating peak ozone mixing ratios is found to be varying from

183 about -26% (7th Jun) to +21% (9th May). The biases are found to be within the variability of 1 stan-

184 dard deviation in 10–12 km altitude (28–59 nmol mol^{-1}) as calculated from ozonesonde observations

185 during spring over this site (See Table 1 and Ojha et al. (2014)).

186 However, the model generally overestimates the ozone mixing ratios in the lower troposphere by

187 about 11–24 nmol mol^{-1} (Table 1) and shows some limitation in capturing less pronounced SOPs,

188 typically observed outside the winter-spring seasons. The bias in the absolute ozone enhancement

189 (-45 nmol mol^{-1}) as well as in the altitudinal placement of the SOP (by 2 km) are higher on 7th Jun.

190 Here EMAC simulations are evaluated for all events identified visually (Ojha et al., 2014). The SOP

191 events are selected based on specific criteria in order to calculate the frequency of occurrence, as

192 discussed in detail in Sect. 3.3.

193 Possible biases between model and observations could arise from a variety of sources, most impor-

194 tantly, the time-evolution of the SOPs (Supplementary material - Figure S1). Therefore, the limited

195 number of ozone profile measurements could lead to a temporal difference in the state of SOP evo-

196 lution being compared between model and observation. We tried to minimize this effect by applying

197 a weighted average algorithm, as mentioned above.

198   Overall, the model is found to be able of reproducing the occurrence of SOPs, their altitudinal

199   placements and the ozone enhancements over the central Himalayas. Additionally, EMAC simulated

200   average ozone distribution appears to compare well with the ozonesonde climatology over Delhi

201   (77.16^{o}E, 28.49^{o}N) in north India (Fig. S2) and with aircraft-based measurements from the IAGOS-

202   CARIBIC program (Jöckel et al., 2016). Hence, we use the EMAC simulations to investigate the

203   underlying processes (Section 3.2), the frequency of occurrences (Section 3.3) and the effects on

204   tropospheric ozone budget (Section 3.4).

205   **3.2   Origin of SOPs**

206   In this section, we analyze the EMAC simulated meteorological and chemical fields in conjunction

207   with backward air trajectories to investigate the origin of SOPs over the central Himalayas. Fig. 3

208   shows the vertical profiles of potential vorticity (PV), a tracer of stratospheric intrusions, during the

209   SOP events observed over Nainital. PV vertical profiles during all SOPs show layers of high values

210   coinciding with the altitude of SOPs.

211   The enhanced PV layers are found to be weaker during June and October compared to events dur-

212   ing late winter and spring. PV values are found to be between 3.1 PVU (20th Apr) to 4.7 PVU (11th

213   Feb) at the SOP altitudes for the events occurring in winter-spring. Even during the less pronounced

214   events of early-summer and autumn, the PV values at SOP altitude are 1.8–2.5 PVU. Further, the av-

215   erage vertical profile of PV during SOPs, derived from a long-term model simulation (2000–2014),

216   shows similar structure (Supplementary material- Fig. S3), as shown here for the individual events.

217   Average PV values during SOPs are found to be significantly higher (e. g. 3.0±1.3 PVU in winter,

218   1.8±0.5 PVU during summer monsoon) compared to timesteps without SOP (0.3±0.2 – 1.5±1.3

219   PVU) (Supplementary material- Table S1). Such enhanced PV values during the SOPs suggest that

220   the air masses showing very high ozone levels (SOPs) are of stratospheric origin.

221   To quantify the amount of ozone transported from the stratosphere during the SOPs, we compare

222   the EMAC simulated vertical profiles of O_3 with O_3s during observed 6 SOP events (Fig. 4). O_3s

223   values are very similar to O_3 indicating that nearly all the excess ozone that constitutes SOPs is of the

224   stratospheric origin, except on 7th Jun and 25th Oct. The contribution of tropospheric photochemical

225   sources to the SOPs, as represented by the difference O_3-O_3s, is found to be significant on 25th Oct

226   (15 nmol mol^{-1}) and much larger on 7th Jun (50 nmol mol^{-1}).

227   The comparison of O_3 with O_3s is further analyzed for the extended period 2000–2014 and a

228   seasonal climatology is derived by aggregating all SOP events into four different seasons (Fig. 5).

229   The average amount of ozone transported from the stratosphere to the SOPs is found to be the high-

230   est during spring (162.5±40 nmol mol^{-1}), followed by winter (149.4±35 nmol mol^{-1}). In contrast

231   the contribution of tropospheric photochemical sources to the SOPs is highest during the summer

232   monsoon (30 nmol mol^{-1}). The stronger anthropogenic contribution up to (and beyond) the SOP al-

233   titudes during the summer monsoon could be a combined effect of deep convective mixing towards

234 the onset of the summer monsoon and weak horizontal winds (Ojha et al., 2014; Naja et al., 2016)

235 leading to the accumulation of the photochemically processed air masses of tropospheric origin.

236   Since the LRT over this region is located significantly higher (Fig. 4, also see Naja et al. (2016))

237 than the altitude of SOPs, and that the ozone in SOPs is found to be of stratospheric origin, we

238 conclude that stratospheric air masses are sandwiched between tropospheric layers at 10–11 km

239 altitude. This result complements previous studies primarily showing the altitudinal placement of

240 SOPs at about 14 km near the Lower Stratosphere (UTLS) (e.g. Reid and Vaughan, 1991; Hwang

241 et al., 2007).

242   In order to investigate the underlying dynamics that transport the stratospheric air masses, leading

243 to the SOPs over the Himalayas, we analyzed the backward air trajectories (Supplementary material-

244 Fig. S4), initialized over Nainital at 10, 11 and 12 km, which are the typical altitudes of the SOPs

245 (Fig. 2). The air mass trajectories indicate rapid transport from the west, for example on 11th Feb,

246 taking only two days for the air masses to be transported across Africa and Middle-East and reach

247 the Himalayas. Further, the locations of the tropopause folds occurred during the period of air trajec-

248 tories are also shown. The tropopause folds are mostly found in a belt between about 20 and 35°N,

249 in agreement with previous studies (Ŝkerlak et al., 2015). The air masses have been encountering

250 extensive tropopause dynamics along the path of transport, before reaching the Himalayas.

251   Additionally, air mass trajectories were computed for each model timestep during May 2002 in

252 which the frequency of SOPs was found to be the highest during the 2000–2014 period. Fig. 6 shows

253 the EMAC simulated evolution of O_3s along these trajectories classified into SOPs and No SOPs

254 above Nainital. The evolution of O_3 and PV along the trajectories are shown in the supplementary

255 material (Fig. S7 and S8). Air masses are enriched / accumulate the ozone of stratospheric origin

256 during transport to Nainital causing SOPs. A significant fraction of trajectories during non SOP

257 timesteps originates over the south west having lower O_3s (< 90 nmol mol^{-1}). The trajectories which

258 do get higher contributions of stratospheric ozone are found to be diluted during transport, making

259 the enhancements above Nainital too small to be an SOP.

260   The vertical distribution of EMAC simulated O_3s/O_3 ratio along the 5-day backward air trajecto-

261 ries are shown in Fig. 7. The pressure variations of the air masses and tropopause along the trajectory

262 are also shown. The O_3s/O_3 ratio is mostly found to be close to unity ($\geq$0.9) near the altitude (pres-

263 sure) of air mass trajectory during transport, except on 7th Jun and 25th Oct (0.5–0.8). The intrusions

264 enriching tropospheric air masses with stratospheric O_3 are clearly visible. More specifically, a sig-

265 nificant stratospheric contribution to tropospheric ozone is found in the upper/middle troposphere

266 during the 5-day period before the event, with the associated PV values (< 2 pvu) indicating mixing

267 of stratospheric air into the troposphere. Additionally, strong variability in the altitude of the LRT

268 along the path of the transport is seen, except for the event of 7th Jun. The dramatic variability in

269 the LRT along the trajectory (e.g. from 100 to 200 hPa on 11th Feb) appears to be associated with

270 the tropopause folding activity (Fig. S4 and S5). Several shallow tropopause folds (vertical extent

of 50 to 200 hPa) occur along the transport path, while medium folds (vertical extent of 200–350 hPa) are only found during 11th Feb and 9th May. Intrusion of a significant amount of O_3 due to tropopause folds over the Eastern Mediterranean and the Middle-East was shown by Akritidis et al. (2016). The combination of very strong winds associated with the subtropical jets (Fig. S4, (Ojha et al., 2014; Naja et al., 2016)) and this intense tropopause dynamics, enriching the troposphere with stratospheric ozone, leads to the formation of SOPs over the Himalayas.

The transport of ozone rich air masses from the stratosphere towards the Himalayas can be seen more clearly in the longitude-pressure cross sections at 30°N (Fig. 8), and latitude-pressure cross sections at 80°E (Fig. 9) for all the events and the day before. Fig. 8 reveals three geographical regions viz. Northern Africa and Atlantic Ocean (lon < 40°E), Middle-East (40°E–60°E) and northern South Asia (60°E–100°E), where the intrusions of stratospheric air masses can be identified. Blobs of air masses characterized by high PV values (> 2 PVU) are also seen. Additionally, Fig. 9 shows that stratospheric influences are more pronounced over the northern parts of the Indian subcontinent compared to Southern India. This result based on EMAC simulations is found to be in agreement with the study by Ganguly and Tzanis (2011) based on ozonesonde observations at three Indian stations.

To investigate the possible mixing of the transported stratospheric air with tropospheric air in the vicinity of the SOPs, the Turbulence-Index (TI) is derived from EMAC fields, as described in Ellrod and Knapp (1992). To detect the Clear Air Turbulence (CAT) areas and potential mixing, the approach similar to Traub and Lelieveld (2003) has been followed. The pressure-longitude cross sections of O_3s (color filled) and TI (contour lines) at 29.5°N near the SOPs pressure height (400-100 hPa) are shown in the Fig. 10 for the timesteps of events and a timestep before and after the event. The enhanced TI values during the SOP events above Nainital indicate higher probability of mixing between stratospheric and tropospheric air, supporting the irreversible nature of the associated STT.

3.3 Frequency of SOPs

The frequency of SOP occurrences was not estimated over Nainital from observations, due to the availability of only 3-4 profiles in each month, however a tendency of higher frequency during spring was noticed (3 events), as compared to other seasons (1 event per season) (Ojha et al., 2014). In this section, we use long-term EMAC simulations, conducted for a period of 15 years (2000–2014), to investigate the frequency of SOP occurrence and seasonality over the central Himalayas. Due to the variability in the SOP altitude as well as the absolute enhancements during the SOPs, general / unique criteria can not be defined. Therefore, we first select the ozone profiles in which Average Ozone Mixing Ratios (AOMR) at 10–12 km, a typical altitude of SOP occurrence, are significantly higher (at least by 50%) compared to average ozone in the lower troposphere. Additionally, to explicitly select only the profiles which are SOPs (and not a direct intrusion over the Himalayas) the additional criterion was applied that directly above the SOP the ozone mixing ratios are again lower (at least by

307 20%), so that selected profiles have a shape typical of SOPs, as shown in Fig. 2. These two conditions

308 can be mathematically expressed as

309 $AOMR_{10-12km} \geqslant 1.5 \times AOMR_{0-6km}$

310 and

311 $AOMR_{12-14km} \leqslant 0.8 \times AOMR_{10-12km}$

312 Further, the factors 1.5 and 0.8 representing an enhancement by 50% and reduction by 20% were

313 suitably varied, which confirmed the generality of the result (not shown). We calculated the fre-

314 quencies of occurrence in percentage for each month during 2000–2014, and converted these to

315 an average climatological seasonal cycle (Fig. 11). Standard deviations in a month represents the

316 variability in the SOP frequency among different years during 2000-2014 period.

317 The highest frequency of SOPs over the central Himalayas is found during the pre-monsoon sea-

318 son (MAM), followed by winter (DJF). The frequency of SOP occurrences over Nainital increases

319 steadily from January (2.7%) to May (10.8%), and abruptly declines in June (1.2%). The model does

320 not predict any SOPs during July–October. It should be noted that here we included only those events

321 as SOPs, which show enhancements by at least 50%, therefore some events with smaller enhance-

322 ments could be present during July–October. It is suggested that the more frequent stratospheric in-

323 trusions during spring, combined with the stronger horizontal advection, lead to more frequent SOP

324 events. Seasonal composites of the spatial locations of folds (Fig. S6) shows higher frequency of

325 occurrence during SOPs. The effects of stronger cross-tropopause exchange and influx of the strato-

326 spheric air masses during spring and winter over the Himalayas and surrounding regions, such as

327 southern parts of the Tibetan Plateau, have also been shown by Ŝkerlak et al. (2014, 2015). The fre-

328 quency of SOP events over this region is minimum during the summer monsoon season, as the weak

329 horizontal winds (Ojha et al., 2014; Naja et al., 2016) do not transport the ozone from STTs over

330 large distances. The frequency of stratospheric intrusions and tropopause folds over the Himalayas

331 and surrounding regions are lower during the summer monsoon (Cristofanelli et al., 2010; Putero

332 et al., 2016). Multiple tropopauses that can occur in winter and spring over the Tibetan Plateau are

333 shown to be absent during the summer monsoon season (Chen et al., 2011). Additionally, stronger

334 vertical mixing due to monsoonal convection inhibits high ozone layers to form and sustain. These

335 findings are in agreement with the ground-based ozone measurements in the southern Himalaya,

336 where about 78% of the stratospheric influences were attributed to the PV structures induced by

337 fluctuations of the zonal flow and tropopause fold development along the the subtropical jet-stream,

338 while monsoon depressions only account for 3% of the events (Bracci et al., 2012). Further, the

339 seasonality of SOP frequency derived from EMAC simulations is consistent with the conclusions

340 based on the limited number of observational profiles in Ojha et al. (2014). Next we determine the

341 enhancements in tropospheric ozone columns due to presence of SOPs over the central Himalayas.

3.4 Effect of SOPs on Tropospheric Column Ozone

Fig. 12 shows the climatological mean seasonal cycle of the Tropospheric Column Ozone (TCO) in Dobson Units (DU) over Nainital from EMAC simulations over the period 2000–2014. TCO values are calculated by integrating ozone mixing ratios up to the LRT, determined using the WMO definition. To investigate the effect of SOPs on TCO, we compare three TCO values: First using EMAC simulated O_3 values from all time steps, second by selecting only the time steps when there is an SOP event as per the criteria discussed in Sec. 3.3, and third by taking all time steps when SOPs do not occur.

TCO values for All-times and No-SOPs are found to be very similar, mainly due to the large number of data counts (more than 1000 data counts in individual month), as compared to those in SOPs (0-120 data counts in individual month). The maxima of TCO during May and June (54.7±5.9 and 55.0±4.4 DU respectively) are attributed to the intense solar radiation and high pollution loading over northern India. While photochemical production of ozone is less efficient during the winter (TCO: 33.7±3.6 to 37.6±5.8 DU) and the summer monsoon (e.g. 44.9±4.9 DU in August). Overall, the EMAC simulated TCO seasonality from all data is found to be consistent with satellite data (Ojha et al., 2012) over this region.

The occurrences of SOPs are seen to clearly enhance the TCO values during the winter, pre-monsoon and early summer. To estimate the enhancement in the tropospheric ozone that would likely persist in the troposphere (not reversible), here an additional criterion of PV values upto 2 PVU has been applied.

The maximum enhancement in climatological average TCO value due to SOPs is found during January, when TCO values during SOPs (43.5±3.0 DU) are higher by as much as 7.5 DU (21%) compared to the non-SOP time steps (36.0±3.6 DU). The enhancements in tropospheric ozone loading over the central Himalayas due to SOPs are estimated to be 3.3–7.5 DU (6–21%) during January to June. Additional calculations, relaxing the PV criteria to include SOP timesteps having PV values higher than 2PVU as well, shows slightly higher values of the estimated enhancement (4–9 DU: 7–26%) on the TCO.

4 Conclusions

In this study, we used the EMAC model to investigate the layers of high ozone mixing ratios (SOPs) in the middle-upper troposphere, observed over the central Himalayas in northern India. EMAC successfully reproduces the occurrence, altitudinal placement and the relative ozone enhancements during SOP events observed in ozonesonde profiles. The vertical profiles calculated by long-term EMAC simulations show layers of high PV (1.8±0.5 – 3.0±1.3 PVU) coinciding with the altitude of SOPs suggesting the influences from stratospheric intrusions. The analysis of O_3s further shows that generally all excess ozone at SOP altitudes over the Himalayas is transported from the stratosphere.

377 Average O_3s at the SOP altitudes is estimated to be maximum during the spring (162.5 ± 40 nmol
378 mol^{-1}), followed by winter (149.4 ± 35 nmol mol^{-1}). Tropospheric photochemical sources are found
379 to contribute significantly to the SOPs and above during the summer monsoon (30 nmol mol^{-1}).

380 Analysis of backward air trajectories in conjunction with EMAC simulated O_3 distributions and
381 tropopause dynamics revealed that stratospheric air masses are sandwiched between tropospheric
382 layers at 10–11 km altitude due to tropopause folds which are rapidly transported along the sub-
383 tropical jet to cause SOP structures over the Himalayas. In contrast to SOP timesteps, a fraction of
384 air mass trajectories during non SOP timesteps are from the south west, which have significantly
385 lower contributions of stratospheric ozone. Regions as far as northern Africa and the Atlantic Ocean,
386 the Middle-East and northern South Asia are found to be regions of stratospheric intrusions that act
387 as sources of high-ozone mixing ratios. The distribution of O_3s showed that STT effects are more
388 pronounced over the northern Indian subcontinent than those over southern India.

389 We used long-term model simulations (2000–2014) to calculate the frequency of SOP occurrence
390 showing maxima during spring (about 11% of the time in May), while no SOPs were predicted
391 during the July–October months. This is consistent with results based on ozone soundings over the
392 region. The high frequency of SOPs during spring is attributed to the occurrence of stratospheric
393 intrusions combined with rapid horizontal transport. The minima in the frequency of SOPs during
394 the summer monsoon are partially due to much weaker horizontal transport due to the northward
395 displacement of subtropical jet stream and stronger monsoonal convective mixing. Model simula-
396 tions were further used to investigate the effect of SOPs on the TCO. The EMAC simulated TCO
397 seasonality is in agreement with satellite data. SOP occurrence is found to significantly enhance the
398 TCO over the region by 3.3–7.5 DU (6–21%). Such an enhancement in tropospheric ozone at the
399 SOP altitude could translate to an increase in surface temperature by 0.06 to 0.13 degree, based on
400 the vertical profile of ozone forcing (Lacis et al., 1990). Additionally, as expected due to their origin
401 from dynamical processes, the occurrences of SOPs discern very large interannual variability (see e.
402 g. Supplementary material-Fig. S9), which highlights a need of in situ measurements and numerical
403 simulations on climatic timescales to quantify the role of SOPs in measured ozone trends over Asian
404 regions especially in the middle-upper troposphere (Banerjee et al., 2016; Tanimoto et al., 2016),
405 and their impacts on tropospheric chemistry and climate.

406 *Acknowledgements.* The model simulations have been performed at the German Climate Computing Centre
407 (DKRZ) through support from the Bundesministerium für Bildung und Forschung (BMBF). DKRZ and its
408 scientific steering committee are gratefully acknowledged for providing the HPC and data archiving resources
409 for this consortial project ESCiMo (Earth System Chemistry integrated Modelling). The authors gratefully ac-
410 knowledge the NOAA Air Resources Laboratory (ARL) for the provision of the HYSPLIT transport and disper-
411 sion model and READY website (http://www.ready.noaa.gov) used in this publication. Constructive comments
412 and suggestions from the two anonymous reviewers are gratefully acknowledged.

References

Akritidis, D., Pozzer, A., Zanis, P., Tyrlis, E., Škerlak, B., Sprenger, M., and Lelieveld, J.: On the role of tropopause folds in summertime tropospheric ozone over the eastern Mediterranean and the Middle East, Atmospheric Chemistry and Physics Discussions, 2016, 1–24, doi:10.5194/acp-2016-547, http://www.atmos-chem-phys-discuss.net/acp-2016-547/, 2016.

Banerjee, A., Maycock, A. C., Archibald, A. T., Abraham, N. L., Telford, P., Braesicke, P., and Pyle, J. A.: Drivers of changes in stratospheric and tropospheric ozone between year 2000 and 2100, Atmospheric Chemistry and Physics, 16, 2727–2746, doi:10.5194/acp-16-2727-2016, http://www.atmos-chem-phys.net/16/2727/2016/, 2016.

Bracci, A., Cristofanelli, P., Sprenger, M., Bonafè, U., Calzolari, F., Duchi, R., Laj, P., Marinoni, A., Roccato, F., Vuillermoz, E., and Bonasoni, P.: Transport of Stratospheric Air Masses to the Nepal Climate Observatory–Pyramid (Himalaya; 5079 m MSL): A Synoptic-Scale Investigation, Journal of Applied Meteorology and Climatology, 51, 1489–1507, doi:10.1175/JAMC-D-11-0154.1, 2012.

Chen, X. L., Ma, Y. M., Kelder, H., Su, Z., and Yang, K.: On the behaviour of the tropopause folding events over the Tibetan Plateau, Atmospheric Chemistry and Physics, 11, 5113–5122, doi:10.5194/acp-11-5113-2011, http://www.atmos-chem-phys.net/11/5113/2011/, 2011.

Cristofanelli, P., Bracci, A., Sprenger, M., Marinoni, A., Bonafè, U., Calzolari, F., Duchi, R., Laj, P., Pichon, J. M., Roccato, F., Venzac, H., Vuillermoz, E., and Bonasoni, P.: Tropospheric ozone variations at the Nepal Climate Observatory-Pyramid (Himalayas, 5079 m a.s.l.) and influence of deep stratospheric intrusion events, Atmospheric Chemistry and Physics, 10, 6537–6549, doi:10.5194/acp-10-6537-2010, http://www.atmos-chem-phys.net/10/6537/2010/, 2010.

Das, S. S., Ratnam, M. V., Uma, K. N., Subrahmanyam, K. V., Girach, I. A., Patra, A. K., Aneesh, S., Suneeth, K. V., Kumar, K. K., Kesarkar, A. P., Sijikumar, S., and Ramkumar, G.: Influence of tropical cyclones on tropospheric ozone: possible implications, Atmospheric Chemistry and Physics, 16, 4837–4847, doi:10.5194/acp-16-4837-2016, http://www.atmos-chem-phys.net/16/4837/2016/, 2016.

Dee, D. P., Uppala, S. M., Simmons, A. J., Berrisford, P., Poli, P., Kobayashi, S., Andrae, U., Balmaseda, M. A., Balsamo, G., Bauer, P., Bechtold, P., Beljaars, A. C. M., van de Berg, L., Bidlot, J., Bormann, N., Delsol, C., Dragani, R., Fuentes, M., Geer, A. J., Haimberger, L., Healy, S. B., Hersbach, H., Hólm, E. V., Isaksen, L., Kållberg, P., Köhler, M., Matricardi, M., McNally, A. P., Monge-Sanz, B. M., Morcrette, J.-J., Park, B.-K., Peubey, C., de Rosnay, P., Tavolato, C., Thépaut, J.-N., and Vitart, F.: The ERA-Interim reanalysis: configuration and performance of the data assimilation system, Quarterly Journal of the Royal Meteorological Society, 137, 553–597, doi:10.1002/qj.828, http://dx.doi.org/10.1002/qj.828, 2011.

Dobson, G.: The laminated structure of the ozone in the atmosphere, Quarterly Journal of the Royal Meteorological Society, 99, 599–607, 1973.

Draxler, R. and Hess, G.: Description of the HYSPLIT 4 modeling system, NOAA Tech. Memo. ERL ARL-224, NOAA Air Resources Laboratory, Silver Spring, MD, p. 24 pp., 1997.

Draxler, R. and Hess, G.: An overview of the HYSPLIT 4 modeling system of trajectories, dispersion, and deposition, Aust. Meteor. Mag., 47, 295–308, 1998.

Draxler, R., Stunder, B., Rolph, G., Stein, A., and Taylor, A.: HYSPLIT4 USER's GUIDE, http://www.arl.noaa.gov/documents/reports/hysplit_user_guide.pdf, 2014.

Ellrod, G. and Knapp, D.: An Objective Clear-Air Turbulence Forecasting Technique: Verification and Operational Use, Weather and Forecasting, 7, 150–165, doi:10.1175/1520-0434(1992)007<0150:AOCATF>2.0.CO;2, http://dx.doi.org/10.1175/1520-0434(1992)007<0150:AOCATF>2.0.CO;2, 1992.

Fadnavis, S., Chakraborty, T., and Beig, G.: Seasonal stratospheric intrusion of ozone in the upper troposphere over India, Annales Geophysicae, 28, 2149–2159, doi:10.5194/angeo-28-2149-2010, http://www.ann-geophys.net/28/2149/2010/, 2010.

Fishman, J., Wozniak, A. E., and Creilson, J. K.: Global distribution of tropospheric ozone from satellite measurements using the empirically corrected tropospheric ozone residual technique: Identification of the regional aspects of air pollution, Atmospheric Chemistry and Physics, 3, 893–907, doi:10.5194/acp-3-893-2003, http://www.atmos-chem-phys.net/3/893/2003/, 2003.

Ganguly, N. D. and Tzanis, C.: Study of Stratosphere-troposphere exchange events of ozone in India and Greece using ozonesonde ascents, Meteorological Applications, 18, 467–474, doi:10.1002/met.241, http://dx.doi.org/10.1002/met.241, 2011.

Holton, J. R. and Lelieveld, J.: Stratosphere-Troposphere Exchange and its role in the budget of tropospheric ozone, pp. 173–190, Springer Berlin Heidelberg, Berlin, Heidelberg, doi:10.1007/978-3-642-61051-6_8, http://dx.doi.org/10.1007/978-3-642-61051-6_8, 1996.

Hwang, S.-H., Kim, J., Won, Y.-I., Cho, H. K., Kim, J. S., Lee, D.-H., Cho, G.-R., and Oh, S. N.: Statistical characteristics of secondary ozone density peak observed in Korea, Advances in Space Research, 36, 952–957, doi:http://dx.doi.org/10.1016/j.asr.2005.05.080, http://www.sciencedirect.com/science/article/pii/S027311770500699X, 2005.

Hwang, S.-H., Kim, J., and Cho, G.-R.: Observation of secondary ozone peaks near the tropopause over the Korean peninsula associated with stratosphere-troposphere exchange, Journal of Geophysical Research: Atmospheres, 112, n/a–n/a, doi:10.1029/2006JD007978, http://dx.doi.org/10.1029/2006JD007978, d16305, 2007.

Jöckel, P., Kerkweg, A., Pozzer, A., Sander, R., Tost, H., Riede, H., Baumgaertner, A., Gromov, S., and Kern, B.: Development cycle 2 of the Modular Earth Submodel System (MESSy2), Geoscientific Model Development, 3, 717–752, doi:10.5194/gmd-3-717-2010, http://www.geosci-model-dev.net/3/717/2010/, 2010.

Jöckel, P., Tost, H., Pozzer, A., Kunze, M., Kirner, O., Brenninkmeijer, C. A. M., Brinkop, S., Cai, D. S., Dyroff, C., Eckstein, J., Frank, F., Garny, H., Gottschaldt, K.-D., Graf, P., Grewe, V., Kerkweg, A., Kern, B., Matthes, S., Mertens, M., Meul, S., Neumaier, M., Nützel, M., Oberländer-Hayn, S., Ruhnke, R., Runde, T., Sander, R., Scharffe, D., and Zahn, A.: Earth System Chemistry integrated Modelling (ESCiMo) with the Modular Earth Submodel System (MESSy) version 2.51, Geoscientific Model Development, 9, 1153–1200, doi:10.5194/gmd-9-1153-2016, http://www.geosci-model-dev.net/9/1153/2016/, 2016.

Kumar, A., Ram, K., and Ojha, N.: Variations in carbonaceous species at a high-altitude site in western India: Role of synoptic scale transport, Atmospheric Environment, pp. –, doi:http://dx.doi.org/10.1016/j.atmosenv.2015.07.039, http://www.sciencedirect.com/science/article/pii/S1352231015302387, 2015.

Lacis, A. A., Wuebbles, D. J., and Logan, J. A.: Radiative forcing of climate by changes in the vertical distribution of ozone, Journal of Geophysical Research: Atmospheres, 95, 9971–9981, doi:10.1029/JD095iD07p09971, http://dx.doi.org/10.1029/JD095iD07p09971, 1990.

Lal, S., Venkataramani, S., Srivastava, S., Gupta, S., Mallik, C., Naja, M., Sarangi, T., Acharya, Y. B., and Liu, X.: Transport effects on the vertical distribution of tropospheric ozone over the tropical marine regions surrounding India, Journal of Geophysical Research: Atmospheres, 118, 1513–1524, doi:10.1002/jgrd.50180, http://dx.doi.org/10.1002/jgrd.50180, 2013.

Lelieveld, J. and Dentener, F. J.: What controls tropospheric ozone?, Journal of Geophysical Research: Atmospheres, 105, 3531–3551, doi:10.1029/1999JD901011, http://dx.doi.org/10.1029/1999JD901011, 2000.

Lemoine, R.: Secondary maxima in ozone profiles, Atmospheric Chemistry and Physics, 4, 1085–1096, doi:10.5194/acp-4-1085-2004, http://www.atmos-chem-phys.net/4/1085/2004/, 2004.

Logan, J. A.: Tropospheric ozone: :Seasonal behavior, trends and antropogenic influence, J. Geophys. Res., 90, 10 463–10 482, 1985.

Logan, J. A.: Trends in the vertical distribution of ozone: an analysis of ozonesonde data, J. Geophys. Res., 99, 25 553–25 585, 1994.

Mandal, T. K., Cho, J. Y. N., Rao, P. B., Jain, A. R., Peshin, S. K., Srivastava, S. K., Bohra, A. K., and Mitra, A. P.: Stratosphere-troposphere ozone exchange observed with the Indian MST radar and a simultaneous balloon-borne ozonesonde, Radio Science, 33, 861–893, doi:10.1029/97RS03553, http://dx.doi.org/10.1029/97RS03553, 1998.

Monks, P. S., Archibald, A. T., Colette, A., Cooper, O., Coyle, M., Derwent, R., Fowler, D., Granier, C., Law, K. S., Mills, G. E., Stevenson, D. S., Tarasova, O., Thouret, V., von Schneidemesser, E., Sommariva, R., Wild, O., and Williams, M. L.: Tropospheric ozone and its precursors from the urban to the global scale from air quality to short-lived climate forcer, Atmospheric Chemistry and Physics, 15, 8889–8973, doi:10.5194/acp-15-8889-2015, http://www.atmos-chem-phys.net/15/8889/2015/, 2015.

Myhre, G., Shindell, D., Breon, F.-M., Collins, W., Fuglestvedt, J., Huang, J., Koch, D., Lamarque, J.-F., Lee, D., Mendoza, B., Nakajima, T., Robock, A., Stephens, G., Takemura, T., and Zhang, H.: Anthropogenic and Natural Radiative Forcing. In: Climate Change 2013: The Physical Science Basis. Contribution of Working Group I to the Fifth Assessment Report of the Intergovernmental Panel on Climate Change [Stocker, T.F., D. Qin, G.-K. Plattner, M. Tignor, S.K. Allen, J. Boschung, A. Nauels, Y. Xia, V. Bex and P.M. Midgley (eds.)], Cambridge University Press, https://www.ipcc.ch/pdf/assessment-report/ar5/wg1/WG1AR5_Chapter08_FINAL.pdf, 2013.

Naja, M., Bhardwaj, P., Singh, N., Kumar, P., Kumar, R., Ojha, N., Sagar, R., Satheesh, S. K., Krishna Moorthy, K., and Kotamarthi, V. R.: High-frequency vertical profiling of meteorological parameters using AMF1 facility during RAWEX-GVAX at ARIES, Nainital, Curr. Sci., 110, 2317–2325, doi:10.18520/cs/v110/i12/2317-2325, 2016.

Neu, J. L., Flury, T., Manney, G. L., Santee, M. L., Livesey, N. J., and Worden, J.: Tropospheric ozone variations governed by changes in stratospheric circulation, NATURE GEOSCIENCE, 7, 340–344, doi:10.1038/NGEO2138, 2014.

Ojha, N., Naja, M., Singh, K. P., Sarangi, T., Kumar, R., Lal, S., Lawrence, M. G., Butler, T. M., and Chandola, H. C.: Variabilities in ozone at a semi-urban site in the Indo-Gangetic Plain region: Association with the meteorology and regional processes, Journal of Geophysical Research: Atmospheres, 117, doi:10.1029/2012JD017716, http://dx.doi.org/10.1029/2012JD017716, 2012.

532 Ojha, N., Naja, M., Sarangi, T., Kumar, R., Bhardwaj, P., Lal, S., Venkataramani, S., Sagar, R., Ku-
533   mar, A., and Chandola, H.: On the processes influencing the vertical distribution of ozone over
534   the central Himalayas: Analysis of yearlong ozonesonde observations, Atmospheric Environment,
535   88, 201–211, doi:http://dx.doi.org/10.1016/j.atmosenv.2014.01.031, http://www.sciencedirect.com/science/
536   article/pii/S1352231014000491, 2014.

537 Ojha, N., Pozzer, A., Rauthe-Schöch, A., Baker, A. K., Yoon, J., Brenninkmeijer, C. A. M., and Lelieveld,
538   J.: Ozone and carbon monoxide over India during the summer monsoon: regional emissions and trans-
539   port, Atmospheric Chemistry and Physics, 16, 3013–3032, doi:10.5194/acp-16-3013-2016, http://www.
540   atmos-chem-phys.net/16/3013/2016/, 2016.

541 Park, S. S., Kim, J., Cho, H. K., Lee, H., Lee, Y., and Miyagawa, K.: Sudden increase in the total ozone density
542   due to secondary ozone peaks and its effect on total ozone trends over Korea, Atmospheric Environment,
543   47, 226 – 235, doi:http://dx.doi.org/10.1016/j.atmosenv.2011.11.011, http://www.sciencedirect.com/science/
544   article/pii/S1352231011011745, 2012.

545 Pozzer, A., Jöckel, P., Tost, H., Sander, R., Ganzeveld, L., Kerkweg, A., and Lelieveld, J.: Simulating organic
546   species with the global atmospheric chemistry general circulation model ECHAM5/MESSy1: a comparison
547   of model results with observations, Atmospheric Chemistry and Physics, 7, 2527–2550, doi:10.5194/acp-7-
548   2527-2007, http://www.atmos-chem-phys.net/7/2527/2007/, 2007.

549 Pozzer, A., Pollmann, J., Taraborrelli, D., Jöckel, P., Helmig, D., Tans, P., Hueber, J., and Lelieveld, J.: Observed
550   and simulated global distribution and budget of atmospheric C_2–C_5 alkanes, Atmospheric Chemistry and
551   Physics, 10, 4403–4422, doi:10.5194/acp-10-4403-2010, http://www.atmos-chem-phys.net/10/4403/2010/,
552   2010.

553 Pozzer, A., de Meij, A., Pringle, K. J., Tost, H., Doering, U. M., van Aardenne, J., and Lelieveld, J.: Dis-
554   tributions and regional budgets of aerosols and their precursors simulated with the EMAC chemistry-
555   climate model, Atmospheric Chemistry and Physics, 12, 961–987, doi:10.5194/acp-12-961-2012, http:
556   //www.atmos-chem-phys.net/12/961/2012/, 2012.

557 Putero, D., Cristofanelli, P., Sprenger, M., Škerlak, B., Tositti, L., and Bonasoni, P.: STEFLUX, a tool for in-
558   vestigating stratospheric intrusions: application to two WMO/GAW global stations, Atmospheric Chemistry
559   and Physics Discussions, 2016, 1–23, doi:10.5194/acp-2016-514, http://www.atmos-chem-phys-discuss.net/
560   acp-2016-514/, 2016.

561 Ramanathan, V., Ramana, M. V., Roberts, G., Kim, D., Corrigan, C., Chung, C., and Winker, D.: Warming
562   trends in Asia amplified by brown cloud solar absorption, Nature, 448, doi:10.1038/nature06019, http://dx.
563   doi.org/10.1038/nature06019, 2007.

564 Ramanathan, V., Agrawal, M., Akimoto, H., Aufhammer, M., Devotta, S., Emberson, L., Hasnain, S. I., Iyn-
565   gararasan, M., Jayaraman, A., Lawrance, M., Nakajima, T., Oki, T., Rodhe, H., Ruchirawat, M., Tan, S. K.,
566   Vincent, J., Y., W. J., Yang, D., Zhang, Y. H., Autrup, H., Barregard, L., Bonasoni, P., Brauer, M., Brunekreef,
567   B., Carmichael, G., Chung, C. E., Dahe, J., Feng, Y., Fuzzi, S., Gordon, T., Gosain, A. K., Htun, N., Kim, J.,
568   Mourato, S., Naeher, L., Navasumrit, P., Ostro, B., Panwar, T., Rahman, M. R., Ramana, M. V., Rupakheti,
569   M., Settachan, D., Singh, A. K., Helen, G. S., Tan, P. V., Viet, P. H., Yinlong, J., Yoon, S. C., Chang, W.-C.,
570   Wang, X., Zelikoff, J., and Zhu, A.: Atmospheric Brown Clouds: Regional Assessment Report with Focus
571   on Asia, United Nations Environment Programme, Nairobi, Kenya., 2008.

Reid, S. J. and Vaughan, G.: Lamination in ozone profiles in the lower stratosphere, Quarterly Journal of the
Royal Meteorological Society, 117, 825–844, 1991.

Roeckner, E., Brokopf, R., Esch, M., Giorgetta, M., Hagemann, S., Kornblueh, L., Manzini, E., Schlese, U., and
Schulzweida, U.: Sensitivity of Simulated Climate to Horizontal and Vertical Resolution in the ECHAM5
Atmosphere Model, Journal of Climate, 19, 3771–3791, doi:10.1175/JCLI3824.1, http://dx.doi.org/10.1175/
JCLI3824.1, 2006.

Roelofs, G.-J. and Lelieveld, J.: Model study of the influence of cross-tropopause O3 transports on tropo-
spheric O3 levels, Tellus B, 49, 38–55, doi:10.1034/j.1600-0889.49.issue1.3.x, http://dx.doi.org/10.1034/j.
1600-0889.49.issue1.3.x, 1997.

Sarangi, T., Naja, M., Ojha, N., Kumar, R., Lal, S., Venkataramani, S., Kumar, A., Sagar, R., and Chan-
dola, H. C.: First simultaneous measurements of ozone, CO, and NOy at a high-altitude regional repre-
sentative site in the central Himalayas, Journal of Geophysical Research: Atmospheres, 119, 1592–1611,
doi:10.1002/2013JD020631, http://dx.doi.org/10.1002/2013JD020631, 2014.

Shindell, D., Kuylenstierna, J. C. I., Vignati, E., van Dingenen, R., Amann, M., Klimont, Z., Anenberg, S. C.,
Muller, N., Janssens-Maenhout, G., Raes, F., Schwartz, J., Faluvegi, G., Pozzoli, L., Kupiainen, K., Höglund-
Isaksson, L., Emberson, L., Streets, D., Ramanathan, V., Hicks, K., Oanh, N. T. K., Milly, G., Williams, M.,
Demkine, V., and Fowler, D.: Simultaneously Mitigating Near-Term Climate Change and Improving Human
Health and Food Security, Science, 335, 183–189, doi:10.1126/science.1210026, http://science.sciencemag.
org/content/335/6065/183, 2012.

Singh, N., Solanki, R., Ojha, N., Janssen, R. H. H., Pozzer, A., and Dhaka, S. K.: Boundary layer evolu-
tion over the central Himalayas from Radio Wind Profiler and Model Simulations, Atmospheric Chemistry
and Physics Discussions, 2016, 1–33, doi:10.5194/acp-2016-101, http://www.atmos-chem-phys-discuss.net/
acp-2016-101/, 2016.

Sinha, P., Sahu, L., Manchanda, R., Sheel, V., Deushi, M., Kajino, M., Schultz, M., Nagendra, N., Kumar, P.,
Trivedi, D., Koli, S., Peshin, S., Swamy, Y., Tzanis, C., and Sreenivasan, S.: Transport of tropospheric and
stratospheric ozone over India: Balloon-borne observations and modeling analysis, Atmospheric Environ-
ment, 131, 228 – 242, doi:http://dx.doi.org/10.1016/j.atmosenv.2016.02.001, http://www.sciencedirect.com/
science/article/pii/S1352231016300905, 2016.

Ŝkerlak, B., Sprenger, M., and Wernli, H.: A global climatology of stratosphere-troposphere exchange us-
ing the ERA-Interim data set from 1979 to 2011, Atmospheric Chemistry and Physics, 14, 913–937,
doi:10.5194/acp-14-913-2014, http://www.atmos-chem-phys.net/14/913/2014/, 2014.

Ŝkerlak, B., Sprenger, M., Pfahl, S., Tyrlis, E., and Wernli, H.: Tropopause folds in ERA-Interim: Global clima-
tology and relation to extreme weather events, Journal of Geophysical Research: Atmospheres, 120, 4860–
4877, doi:10.1002/2014JD022787, http://dx.doi.org/10.1002/2014JD022787, 2014JD022787, 2015.

Smit, H. G. J., Straeter, W., Johnson, B. J., Oltmans, S. J., Davies, J., Tarasick, D. W., Hoegger, B., Stubi, R.,
Schmidlin, F. J., Northam, T., Thompson, A. M., Witte, J. C., Boyd, I., and Posny, F.: Assessment of the
performance of ECC-ozonesondes under quasi-flight conditions in the environmental simulation chamber:
Insights from the Juelich Ozone Sonde Intercomparison Experiment (JOSIE), Journal of Geophysical Re-
search: Atmospheres, 112, n/a–n/a, doi:10.1029/2006JD007308, http://dx.doi.org/10.1029/2006JD007308,
d19306, 2007.

612 Sprenger, M., Croci Maspoli, M., and Wernli, H.: Tropopause folds and cross-tropopause exchange: A global

613   investigation based upon ECMWF analyses for the time period March 2000 to February 2001, Journal of

614   Geophysical Research: Atmospheres, 108, n/a–n/a, doi:10.1029/2002JD002587, http://dx.doi.org/10.1029/

615   2002JD002587, 8518, 2003.

616 Tanimoto, H., Zbinden, R., Thouret, V., and Nédélec, P.: Consistency of tropospheric ozone observations made

617   by different platforms and techniques in the global databases, Tellus B, 67, http://www.tellusb.net/index.php/

618   tellusb/article/view/27073, 2015.

619 Tanimoto, H., Ikeda, K., Okamoto, S., Thouret, V., Emmons, L., Tilmes, S., and Lamarque, J.-F.: Recent changes

620   in the free tropospheric ozone over East Asian Pacific rim, International Global Atmospheric Chemistry

621   (IGAC) Science Conference, 26-30 September 2016, Breckenridge, CO, USA, http://www.igac2016.org/

622   IGAC2016_Abstracts/5.099_TANIMOTO.pdf, 2016.

623 Traub, M. and Lelieveld, J.: Cross-tropopause transport over the eastern Mediterranean, Journal of Geo-

624   physical Research: Atmospheres, 108, n/a–n/a, doi:10.1029/2003JD003754, http://dx.doi.org/10.1029/

625   2003JD003754, 4712, 2003.

626 Trickl, T., Bärtsch-Ritter, N., Eisele, H., Furger, M., Mücke, R., Sprenger, M., and Stohl, A.: High-ozone layers

627   in the middle and upper troposphere above Central Europe: potential import from the stratosphere along the

628   subtropical jet stream, Atmospheric Chemistry and Physics, 11, 9343–9366, doi:10.5194/acp-11-9343-2011,

629   http://www.atmos-chem-phys.net/11/9343/2011/, 2011.

630 Tyrlis, E., Škerlak, B., Sprenger, M., Wernli, H., Zittis, G., and Lelieveld, J.: On the linkage between the Asian

631   summer monsoon and tropopause fold activity over the eastern Mediterranean and the Middle East, Journal

632   of Geophysical Research: Atmospheres, 119, 3202–3221, doi:10.1002/2013JD021113, http://dx.doi.org/10.

633   1002/2013JD021113, 2014.

634 Varotsos, C., Kalabokas, P., and Chronopoulos, G.: Association of the Laminated Vertical Ozone Structure with

635   the Lower-Stratospheric Circulation, Journal of Applied Meteorology, 33, 473–476, 1994.

636 Venkat Ratnam, M., Ravindra Babu, S., Das, S. S., Basha, G., Krishnamurthy, B. V., and Venkateswararao, B.:

637   Effect of tropical cyclones on the stratosphere-troposphere exchange observed using satellite observations

638   over the north Indian Ocean, Atmospheric Chemistry and Physics, 16, 8581–8591, doi:10.5194/acp-16-8581-

639   2016, http://www.atmos-chem-phys.net/16/8581/2016/, 2016.

Table 1. A comparison of average ozone mixing ratios between ozonesondes and EMAC model for the lower, middle and upper troposphere during the six SOP events over Nainital

Date	2–7 km		7–12 km		12–17 km	
	Sonde	EMAC	Sonde	EMAC	Sonde	EMAC
20110211	50.7±4.1	69.5±3.6	85.8±52.1	112.3±52.3	135.9±22.9	173.7±42.6
20110310	67.6±8.1	86.8±1.8	120.5±52.0	134.8±39.0	131.9±57.4	184.7±76.9
20110420	85.8±7.7	96.9±7.0	147.1±37.3	136.8±28.6	151.4±41.6	151.0±36.7
20110509	83.0±13.3	101.6±5.3	104.8±34.7	154.8±25.3	132.9±15.4	140.7±17.7
20110607	83.1±7.6	107.0±6.1	132.4±30.2	110.2±10.0	119.8±21.6	111.9±35.2
20111025	57.1±3.3	72.3±1.7	84.4±26.8	86.7±17.2	123.3±37.6	130.4±31.7
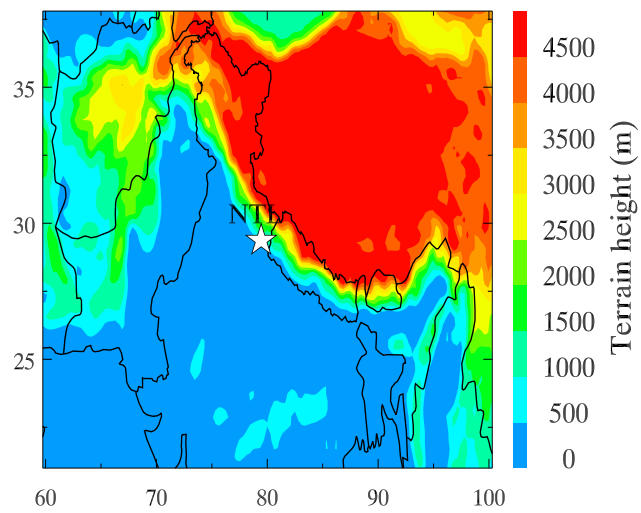
Figure 1. Location of Nainital site in the central Himalayas shown in the topography map of the northern Indian region.
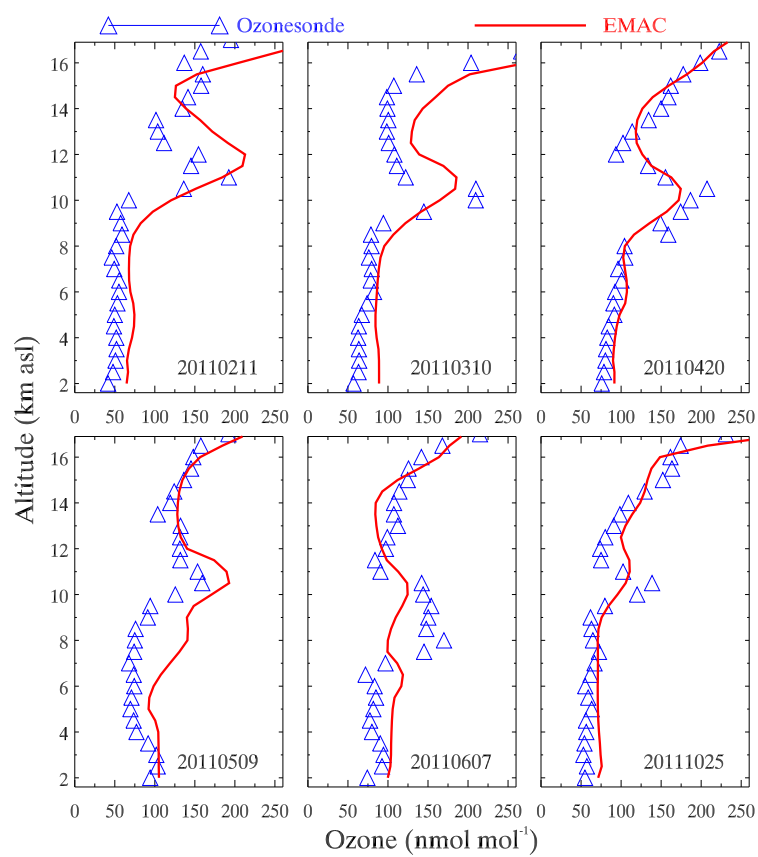
Figure 2. Comparison of EMAC simulated ozone profiles during the days of SOP events with ozonesonde observations over Nainital.
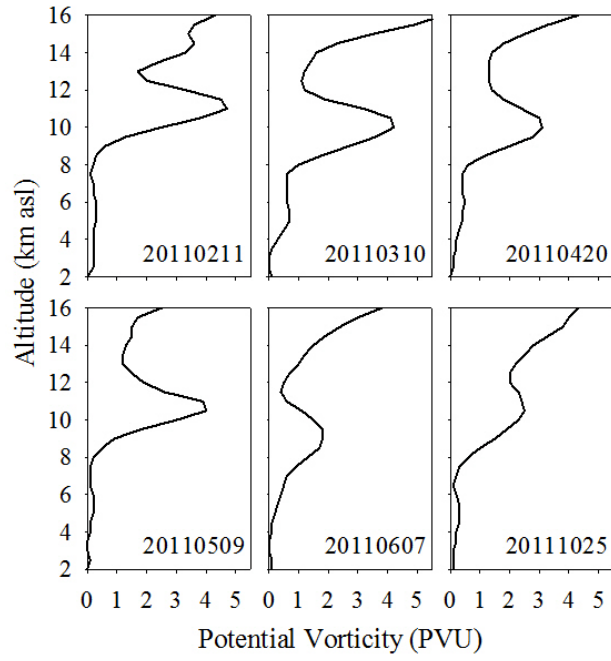
Figure 3. Vertical profiles of potential vorticity (PV) from EMAC simulations during the SOPs over Nainital.
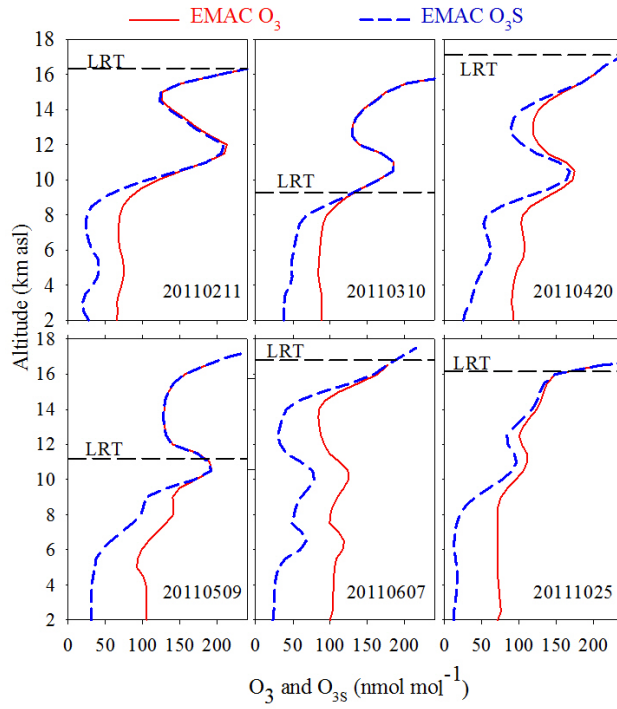
Figure 4. Vertical profiles of EMAC simulated ozone and stratospheric ozone tracer ($O_{3}s$) during the SOPs over Nainital. The height of the Lapse Rate Tropopause (LRT) from EMAC, calculated using the WMO definition, is also shown.
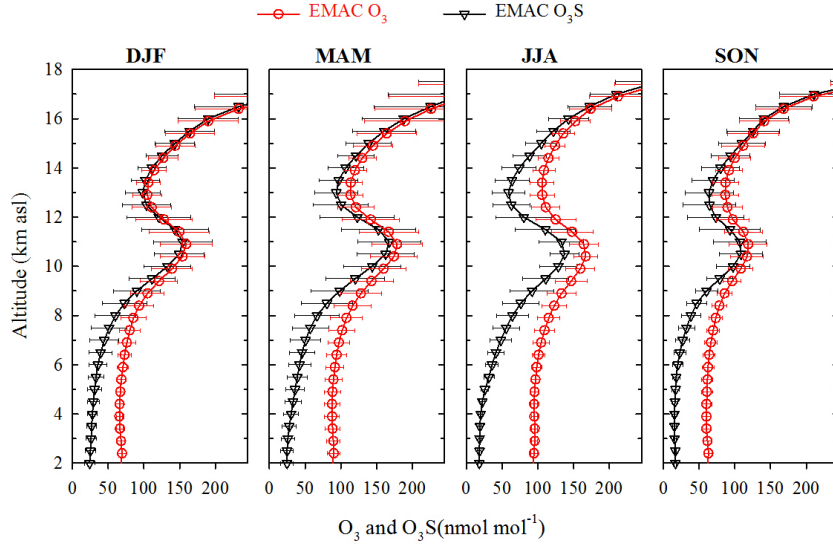
Figure 5. Average vertical profiles of EMAC simulated ozone (O_3) and stratospheric ozone tracer (O_3s) during the SOPs over Nainital aggregated into four seasons: DJF (Winter), MAM (Spring/ pre-monsoon), JJA (summer monsoon), and SON (autumn) for the period 2000–2014.
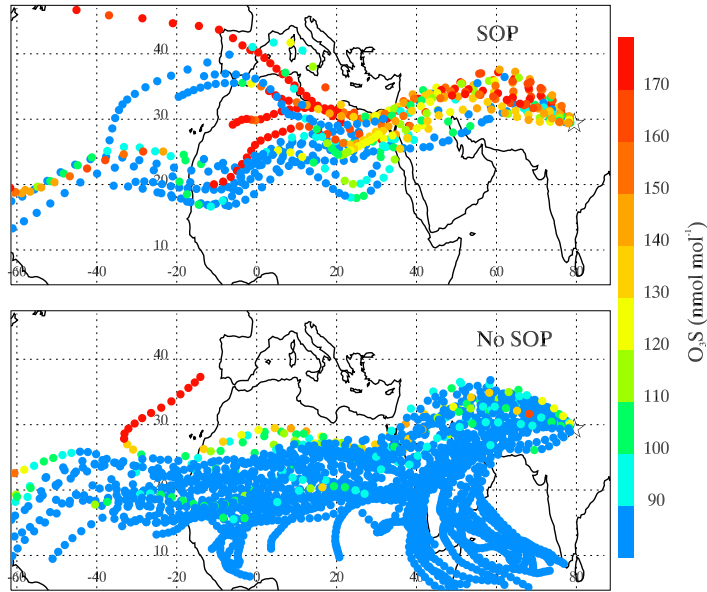
Figure 6. EMAC simulated evolution of O_3s along 5-day backward air trajectories over Nainital during SOPs and No SOPs with starting altitude of 11 km for the month May 2002. The difference between symbols on trajectories represent a time period of 3h. The location of the Nainital site is shown by the star symbol.
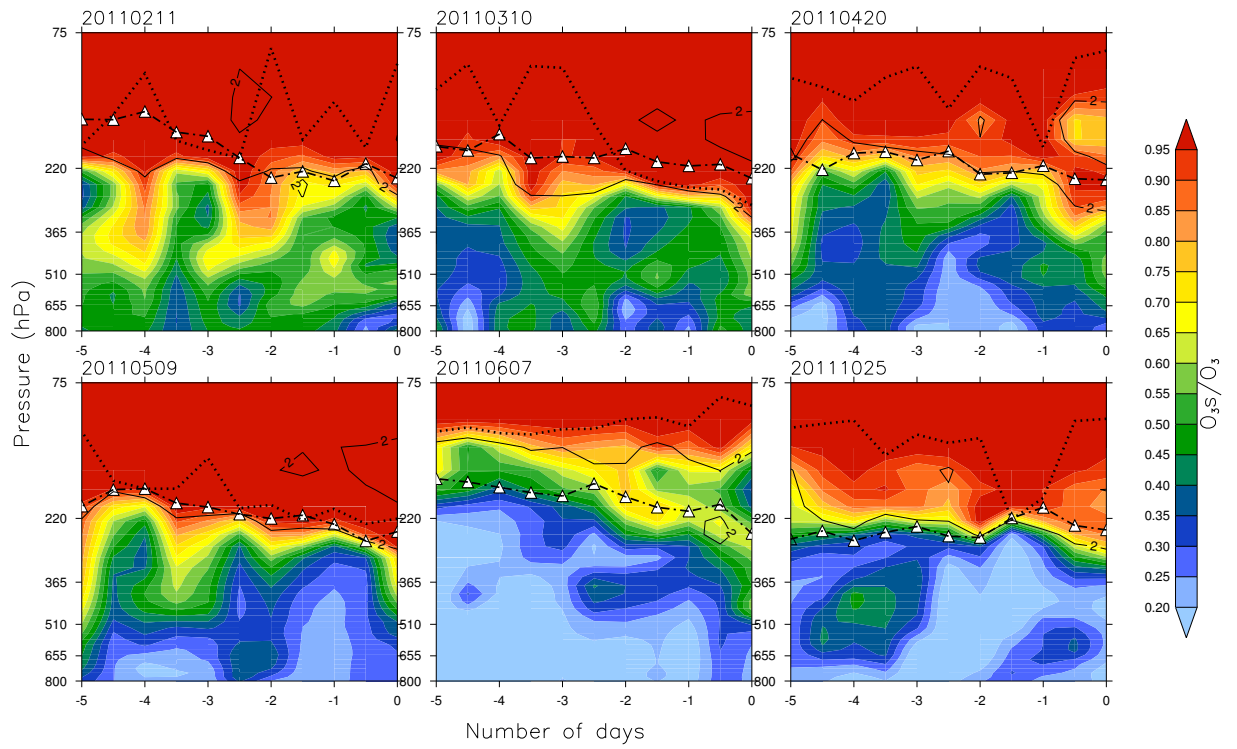
Figure 7. The vertical distribution of EMAC simulated O_3/O_3s ratio along the trajectories with starting altitude of 11km over Nainital. The X axis shows the number of days backward in time and the Y axis shows the pressure in hPa. White filled triangles show the pressure along the back-trajectory and the difference between two consecutive symbols on the line represent a time period of 12 h. The dotted black line indicates the tropopause (LRT). The solid black line is the 2PVU contour.
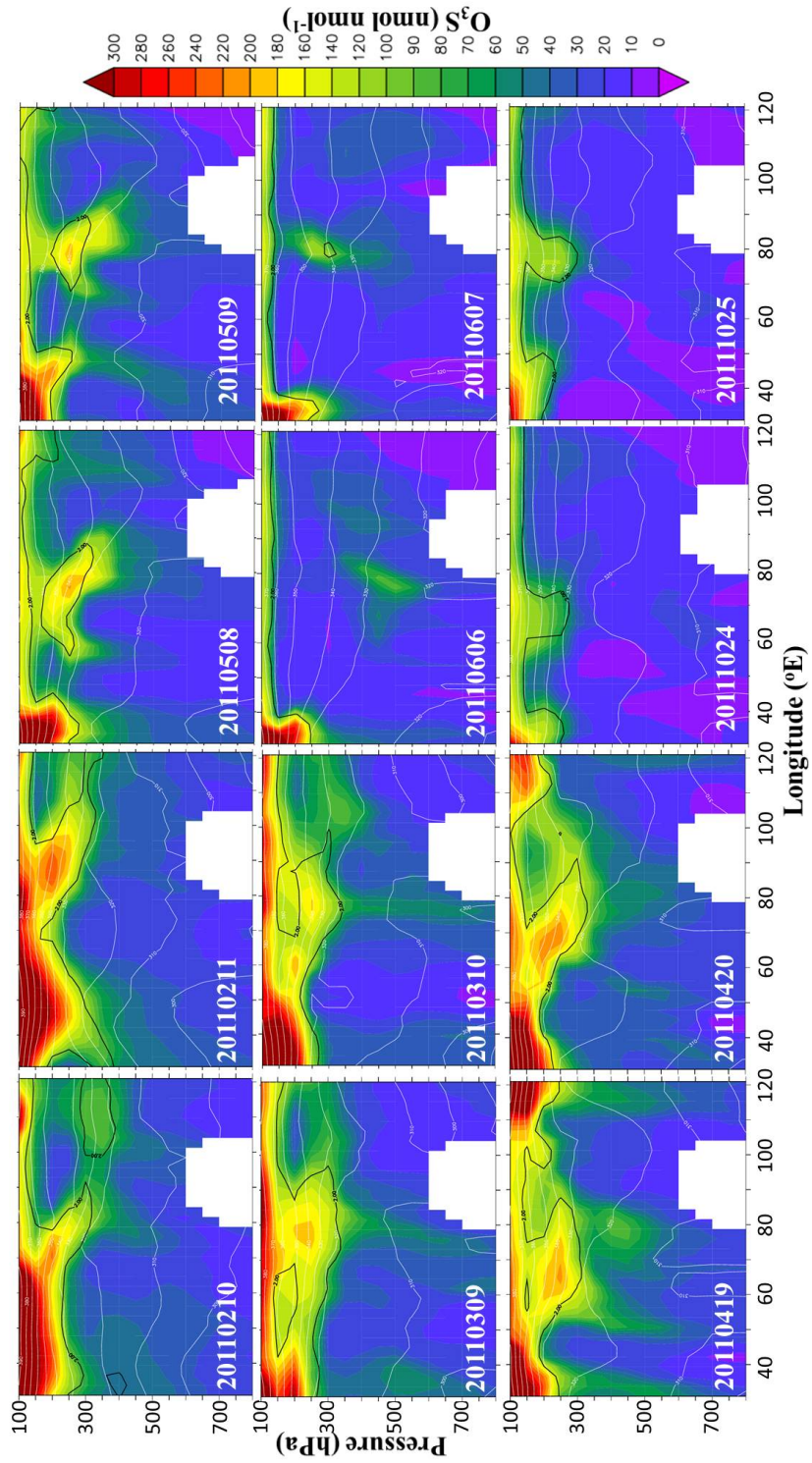
Figure 8. The longitude-pressure cross section of EMAC simulated O_3s at 29.5°N during all SOP days and a day before the event. White lines denote the potential temperature (K) and the black line denotes the dynamical tropopause at 2 PVU.
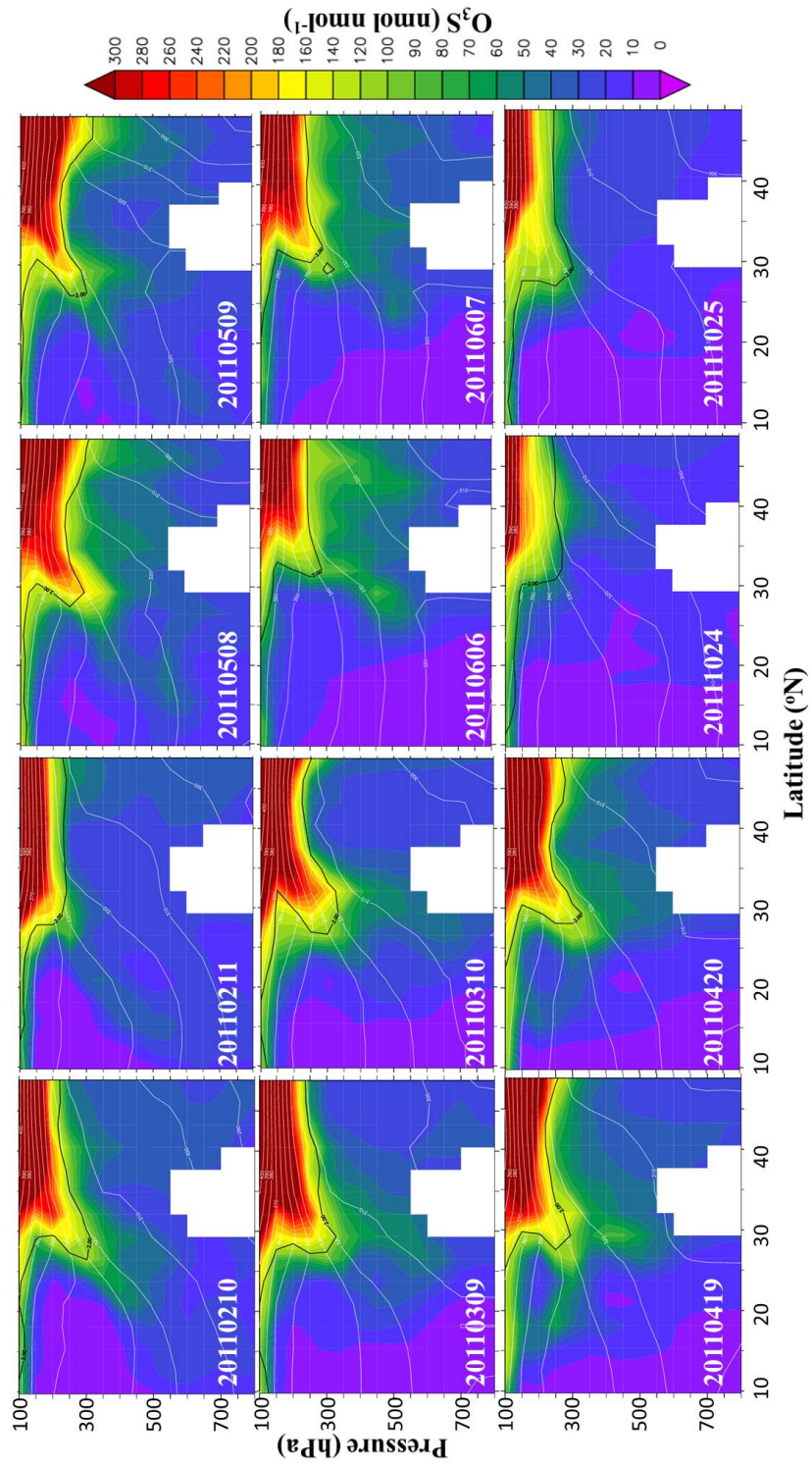
Figure 9. The latitude-pressure cross section of EMAC simulated O₃s at 79.5°E during all SOP days and a day before the event. White lines denote the potential temperature (K) and the black line denotes the dynamical tropopause at 2 PVU.
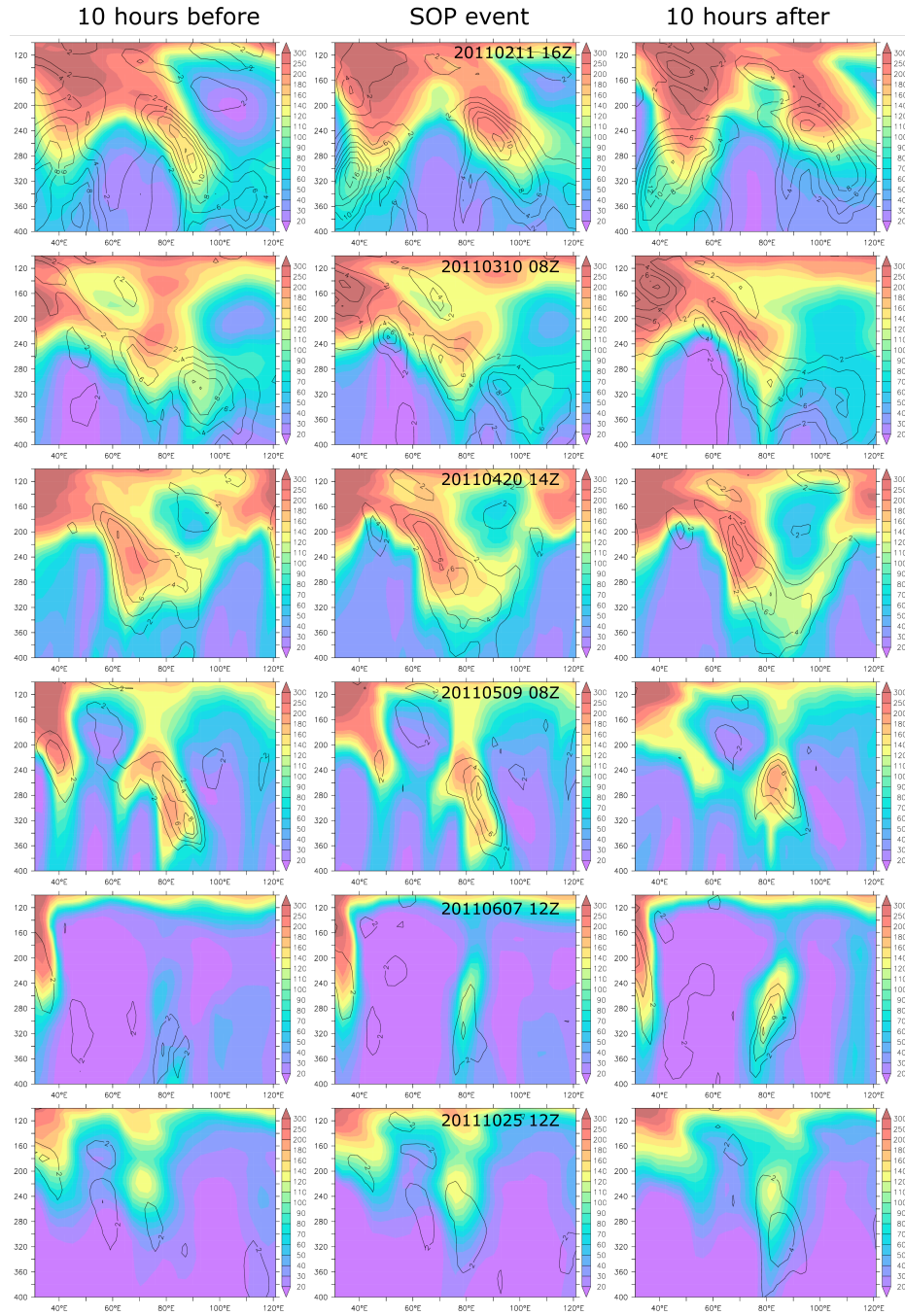
Figure 10. The longitude-pressure cross section of O_3s (color filled), and Turbulence Index (TI) (contour lines) (in $10^{-7}s^{-2}$) at 29.5°N.
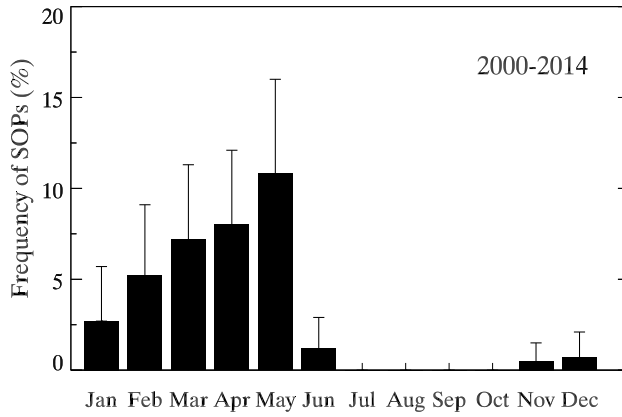
Figure 11. Annual cycle of SOP occurrence frequency (%) over Nainital, calculated from the EMAC simulations for the period 2000–2014. The error bars show the standard deviation of SOP frequency during each month among different years 2000-2014 period.
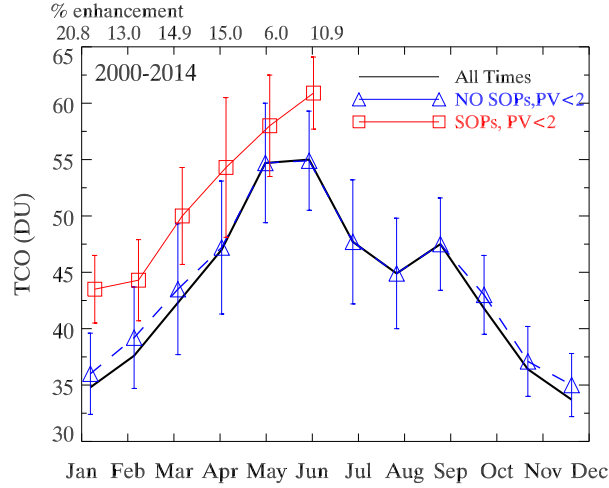
Figure 12. Annual cycle of EMAC simulated TCO over the central Himalayas calculated from 1) all EMAC time steps (All Times), 2) only the time steps having SOPs (SOPs), and 3) only when SOPs are not present (No SOPs) over the period 2000–2014. Enhancements in TCO values (in %) during SOPs as compared to No SOPs are also indicated. TCO values for SOPs and No SOPs are derived only when the average PV value at 10–12 km is up to 2PVU. Error bars represent the standard deviation derived from the temporal variations over the period of 2000-2014.